Reduction of Stator Flux Ripple and Current Harmonic Distortion using Constant Switching Flux Controller-based DTC of Five-Phase Induction Motor

Venkata Subba Reddy C, Swati Devabhaktuni, *Member, IEEE*

***Abstract*— A five-phase induction motor's classical hysteresis-based DTC exhibits excellent dynamics and suffers from higher torque and flux ripple, higher current %THD, and variable switching frequencies that vary with speed. In this article, a triangular-based constant switching flux (CSF) controller is introduced in place of the standard hysteresis-based flux controller without altering the hysteresis-based torque controller for implementing the lookup table-based direct torque control of a five-phase induction motor. The proposed DTC scheme improves the average flux ripple and current harmonic distortion for all operating speeds without altering the superior speed and torque dynamic characteristics as that of the classical DTC scheme. The proposed carrier-based CSF controller smoothens the flux pattern and in turn, improves the current profile with suitable duty variations. The proposed DTC forces flux status change at regular intervals which eliminates the drooping of stator flux under very low speeds and light load cases. The hardware and simulation experimental results are analyzed to know the effectiveness of the proposed constant switching flux controller-hysteresis torque controller-based DTC (CSFHTC-DTC) control scheme over the classical hysteresis flux and hysteresis torque controller-based DTC (HFT-DTC) control scheme with the same lookup table.**

***Index Terms*— Constant switching flux controller, Direct torque control, Flux ripple, Five-phase induction motor, Hysteresis torque controller, Harmonic distortion**

I. INTRODUCTION

Recently, multi-phase electrical machines got good attention in the field of electric automobiles, cruise ships, and electric aircraft due to their overwhelming benefits and the advancement of modern power electronic devices and fast DSP controllers [1], and [2]. In the area of multi-phase machines, several researchers are focused on implementing advanced control strategies for the speed control of five-phase induction motors due to their distinct advantages such as fault-tolerant capability [3], [4], high torque or power density [5], reduced per-phase power, and increased toque pulse frequency and favors smooth drive operation [6]. Advanced control strategies such as predictive torque control scheme, field-oriented control scheme, and direct torque control technique are applied for five-phase induction motors to improve dynamic and steady-state performances [7], and [8]. Recent advancements in multi-phase drive in terms of theoretical explanation, design perception, and modeling are explained in [9], and [10]. The suitability of five-phase induction motors in high-power density applications like ship propulsion, electric vehicles, and spacecraft is discussed in the article [11], and [12]. The conventional DTC scheme gained popularity in industrial applications owing to simplicity and excellent torque dynamics but it exhibits the most common problems like high torque ripple, flux drooping at low speeds, and variable switching frequencies [13]. Detailed analysis of DTC techniques in classical three-phase induction motors is described in [14], [15], which discusses the effects of applied voltage vectors on the developed torque and stator flux under different operating speeds and loads. The analysis done in the [14] and [15] aids the proper selection of voltage vectors in the direct torque control technique of classical three-phase induction motors.

The five-phase voltage source inverter has two independent fundamental space vector (αβ) plane and harmonic space vector (xy) plane components. The fundamental space vector plane (αβ) components are responsible for the production of useful torque and the harmonic plane (xy) components create only ohmic losses and also distort the phase current [16]. Hence, it is necessitating the elimination of harmonic plane components while implementing any control scheme on a voltage source inverter-controlled five-phase induction motor. Hence the DTC control techniques of classical three-phase machines are extended to multi-phase machines with a special concern on harmonic plane components elimination. In literature, numerous literature works have been implemented to control the five-phase induction motor to improve steady-state performance and dynamic performance. Initially, the classical hysteresis-based DTC [17] is implemented on a 2-level inverter-fed five-phase interior permanent magnet drive by applying large switching voltage vectors and medium switching voltage vectors which suffer from shortcomings of classical DTC [13] and lower order harmonic plane components not eliminated. The reference [18], discusses the 3-level hysteresis-based DTC of the five-phase induction motor which eliminates lower order harmonics with the help of the average virtual voltage vector concept and suffers from high torque ripple and variable switching frequency. In reference [19], the same author implemented a five-level DTC on a five-phase induction motor to improve the low-speed performance of the five-phase induction motor with the help of a separate look-up table and mitigate low-frequency harmonics but it suffers from complexity and the existence of small low-frequency components. In reference [20], a modified DTC scheme is implemented to minimize common

mode voltage by employing only large vectors during virtual vectors generation with the expense of higher current %THD. A three-level DTC controller is implemented in [21] for low-speed performance enhancement using an extra lookup table under low speed and still, it exhibits higher flux ripple under low speeds and variable switching frequencies. Reference [22] introduces a three-level five-leg neutral point converter with five and seven-level torque controller-based DTC to decrease torque ripple and flux ripple, which increases system complexity and computational time owing to the use of a neutral point converter and suffers from neutral point balancing issues. Reference [23] and reference [24] implement two different space vector modulated direct torque control (SVM-DTC) algorithms to maintain constant switching frequency, which requires more PI controllers and impacts steady operation at extremely low speeds. The constant switching torque controller introduced in classical DTC in [25] for a three-phase induction motor suffers from sector flux drooping and poor low-speed performance, as well as weak dynamics. A PI torque controller-based constant switching DTC is applied in a three-phase interior PMSM [26] to increase steady-state performance as well as dynamics, but it still exhibits a larger flux ripple owing to the hysteresis flux controller selection. A constant switching torque controller-based DTC (CST-DTC) is implemented in [27] to enhance low-speed performance in terms of torque ripple and still, it suffers from high flux ripple, current %THD, and slow dynamics. In reference [28], a five-level constant switching torque controller is introduced with the help of large and medium voltage vectors to control a five-phase induction motor which exhibits higher flux ripples and poorer dynamic performance, and harmonic plane components are not eliminated.

Most of the literary works on five-phase induction motors focus on torque profile improvement, harmonic plane components elimination, and system dynamics. The proposed work mainly focuses on the improvement of the stator flux pattern and current profile without disturbing the other parameters.

The presented CSFHTC-DTC scheme employed a constant switching flux (CSF) controller and hysteresis torque controllers (HTC) to a voltage source inverter-controlled five-phase induction motor for improving average flux ripple and current harmonic THD without altering faster dynamics of classical hysteresis-based DTC (HFT-DTC) method with the same lookup table. The proposed method mainly concentrates on the reduction of average flux ripple, and current harmonic distortion under different possible rotor speeds with various loads without affecting torque profile and machine dynamics with harmonic plane currents elimination with the concept of virtual voltage vectors.

II. Operation of the Proposed CSFHTC-DTC Method

A 2-level 5-leg inverter generates 32 space voltage vectors and is grouped as large ($0.6472V_{dc}$), medium ($0.4V_{dc}$), small ($0.2472V_{dc}$), and null ($0V_{dc}$) vectors and these vectors are located in both the fundamental (αβ) and harmonic (xy) planes as seen in Fig. 1.

The space voltage vector location can be obtained from (1) and (2) in both fundamental (αβ) and harmonic (xy) planes respectively [27].

$$V_{s(\alpha\beta)} = \frac{2}{5}V_{dc}\left(S_a + S_b e^{j\frac{2\pi}{5}} + S_c e^{j\frac{4\pi}{5}} + S_d e^{j\frac{-4\pi}{5}} + S_e e^{j\frac{-2\pi}{5}}\right) \quad (1)$$

$$V_{s(xy)} = \frac{2}{5}V_{dc}\left(S_a + S_b e^{j\frac{-4\pi}{5}} + S_c e^{j\frac{2\pi}{5}} + S_d e^{j\frac{-2\pi}{5}} + S_e e^{j\frac{4\pi}{5}}\right) \quad (2)$$

Where $V_{s(\alpha\beta)}$=space voltage vector in αβ-plane
$V_{s(xy)}$=space voltage vector in xy-plane
V_{dc}=DC-link voltage of the 5-leg inverter
S_a, S_b, S_c, S_d, S_e=inverter leg switch statuses

From Fig. 1, it is seen that large vectors in the fundamental plane appear as small vectors in the harmonic plane with inverse direction and vice versa and medium vectors in the fundamental plane appear as medium vectors in the harmonic plane [18]. The fundamental plane components are responsible for electromagnetic torque production while the harmonic plane components produce ohmic losses for the distributed winding machine [19].

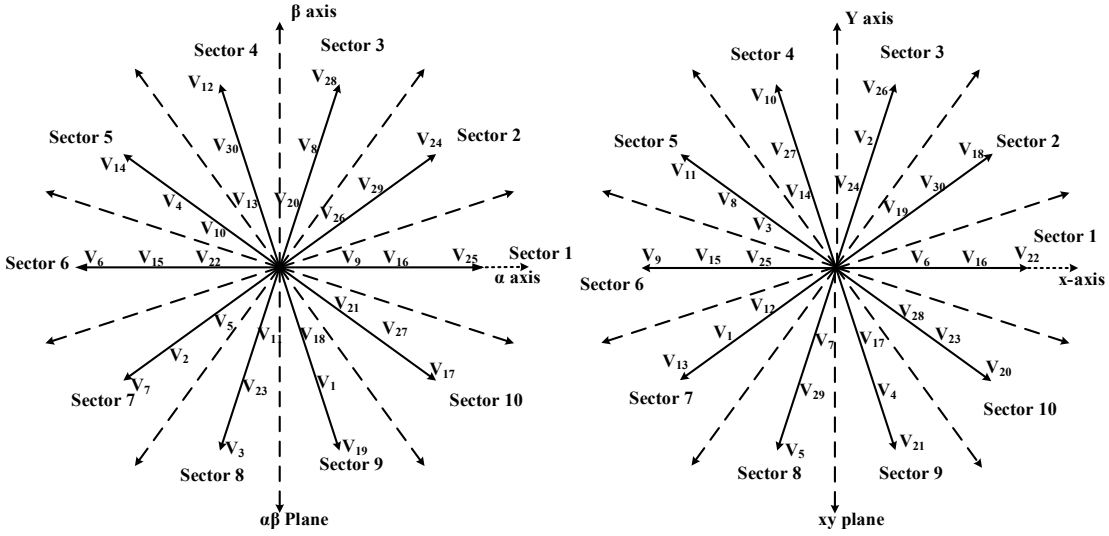

Fig. 1. Space vectors location of the five-phase inverter in fundamental(αβ)-plane and harmonic(xy)-plane.

It is important to eliminate the harmonic plane (xy) components to avoid excessive power loss due to low-frequency harmonic plane currents. The harmonic (xy) plane components are eliminated with the volt-second balancing technique as discussed in [21]. As the amplitude ratio of the medium vector 16 and small vector 25 is 1/0.6181 in the xy plane, the dwell time ratio of the medium vector and small vector states can be set at 0.6181 to make a zero mean volt-second vector in the xy-plane as shown in Fig. 2(b) which eliminates low-frequency harmonic currents [18]. The resultant voltage $V_1(25,16)$ in the fundamental ($\alpha\beta$) plane will be calculated as in (3) and shown in Fig. 2(a).

$$T_s V_1 = t_1 V_L + t_2 V_M$$
$$V_1 = 0.553 V_{dc} \angle 0^0 \quad (3)$$

Where V_M=Magnitude of medium vector=$0.4V_{dc}$
V_L=Magnitude of large vector=$0.642V_{dc}$
t_1 =Dwell time of large vector=$0.618T_s$
t_2 =Dwell time medium vector=$0.382T_s$
T_s=Total sample time=t_1+t_2

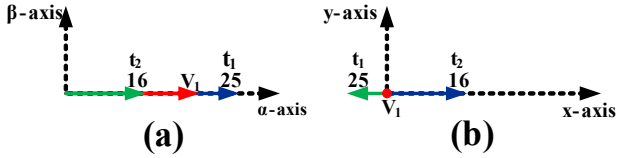

Fig. 2. Resultant virtual voltage vector magnitude (red color) in both (a) αβ-plane (b) xy-plane

The selected inverter switching states with the calculated dwell times form 10 virtual voltage vectors V_1 to V_{10} with a magnitude of $0.553V_{dc}$ in the fundamental plane as shown in Fig. 3. These ten active virtual voltage vectors, as well as the two null voltage vectors V_0 and V_{31} are used to form lookup table for the classical HFT-DTC method and proposed CSFHTC-DTC method. The virtual voltage vector space locus can be divided into 10 sectors as sown in Fig. 3.

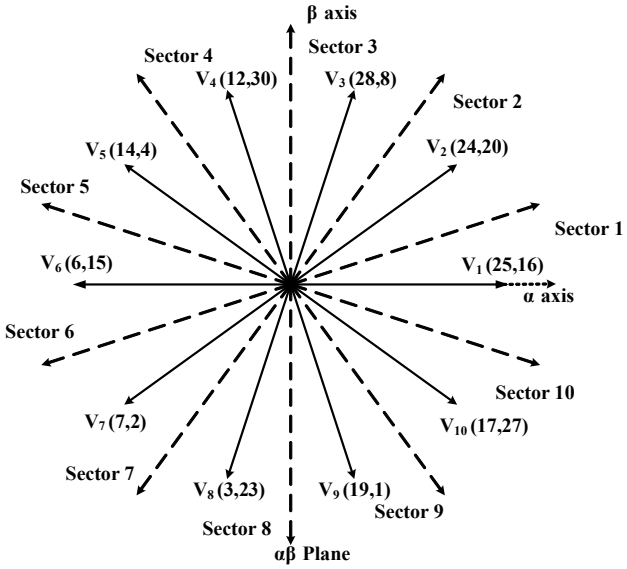

Fig. 3. Space vector diagram of virtual voltage vectors.

The electromagnetic torque (T_e) and stator flux (Ψ_s) are estimated below.

The stator voltage balancing equation in phase manner is written as:

$$V_s = I_s R_s + \frac{d\Psi_s}{dt} \quad (4)$$

Where V_s = stator phase voltage in volts
I_s= stator phase current in amperes
R_s=stator per phase resistance in ohms

The estimated stator flux (Ψ_s) from (4) written as below

$$\Psi_s = \int (V_s - I_s R_s)\, dt \quad (5)$$

The electromagnetic torque (T_e) estimation can be done as (6)

$$T_e = \frac{5}{2}\frac{P}{2} \text{imag}(\Psi_s I_s) \quad (6)$$

Where P- no. of stator poles of five-phase induction motor

Fig. 4 depicts the implementation of the proposed CSFHTC-DTC scheme of a 2-level inverter-controlled five-phase induction motor and the control scheme contains a speed PI controller, speed sensor, hysteresis torque controller, CSF controller, torque-flux estimation block, and switching table. The speed PI controller treats the speed error and generates the reference torque (T_e^*). The estimated stator flux (Ψ_s) and electromagnetic torque (T_e) are compared with the reference torque (T_e^*) and reference flux (Ψ_s^*) respectively, and these errors are processed with a hysteresis torque controller and CSF controller respectively. An appropriate switching state is selected from the lookup table given in Table 1 with the information on torque status (T_{stat}), stator flux status (Ψ_{stat}), and sector number. The selection of switching vectors for control period T_s affects stator flux and torque as seen in (7), and (8).

$$\Delta\Psi_s = (V_s - R_s i_s) T_s \quad (7)$$

$$\Delta Te = \frac{5}{2}\frac{P}{2}\frac{L_m}{L_r L_{ss}} (|\Psi_s + \Delta\Psi_s|)(|\Psi_r|) \sin(\Delta\theta) \quad (8)$$

Where $\Delta\Psi_s$=change in stator flux due to applied voltage in T_s
$\Delta\theta$=change in torque angle due to applied voltage in T_s
ΔT_e=change in torque due to applied voltage in T_s

With the neglected small stator resistance voltage drop in (4), the slope of stator flux can be written as below in (9) and it completely depends on applied voltage vectors.

$$\frac{d\Psi_s}{dt} = V_s \quad (9)$$

The slope of stator flux over T_s is equal to the tangential component of the selected space vector in the locus of stator flux. The positive and negative stator flux slopes for an applied voltage vector within a sector can be written as (10) and (11) respectively.

$$\frac{d\Psi_s^+}{dt} = \frac{2}{5} V_{dc} \sin\theta \quad (10)$$

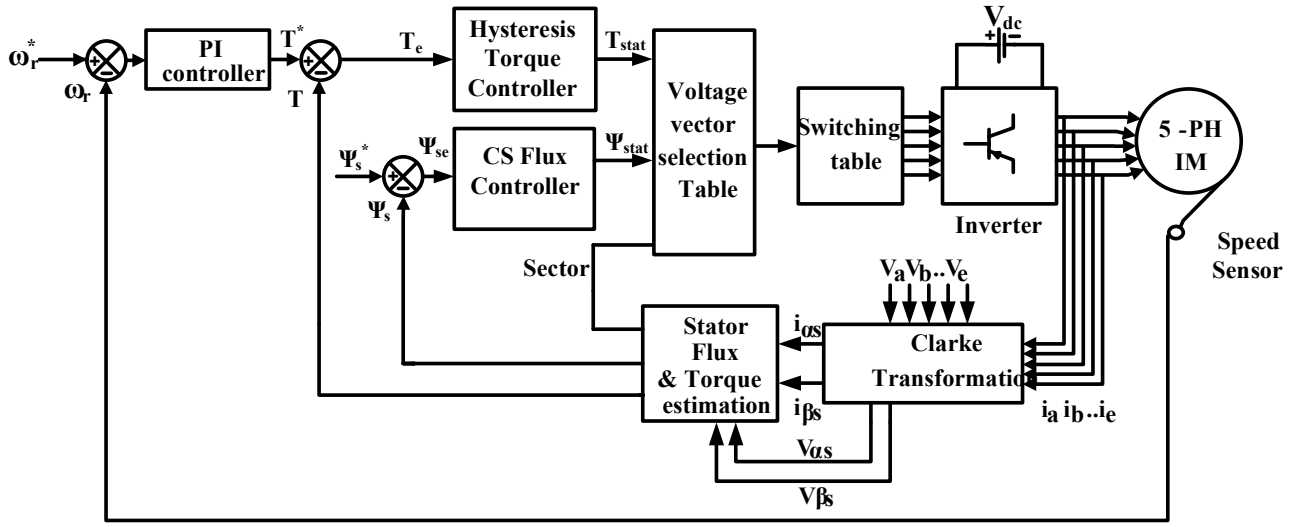

Fig. 4. Implementation of the proposed CSFHTC-DTC control scheme of a five-phase induction motor.

$$\frac{d\Psi_s^-}{dt} = \frac{2}{5}V_{dc}\sin\left(\theta + \frac{4}{5}\pi\right) \quad (11)$$

Where V_{dc}=inverter DC bus voltage
θ =Sector space angle (0 to $\pi/5$)

TABLE I
VECTOR SELECTION TABLE FOR HFT-DTC & CSFHTC-DTC METHODS

Ψ_{stat}	T_{stat}	Sector 1	2	3	4	5	6	7	8	9	10
1	1	V_2	V_3	V_4	V_5	V_6	V_7	V_8	V_9	V_{10}	V_1
1	0	V_0	V_{31}	V_0	V_{31}	V_0	V_{31}	V_0	V_{31}	V_0	V_{31}
1	-1	V_{10}	V_1	V_2	V_3	V_4	V_5	V_6	V_7	V_8	V_9
-1	1	V_5	V_6	V_7	V_8	V_9	V_{10}	V_1	V_2	V_3	V_4
-1	0	V_{31}	V_0	V_{31}	V_0	V_{31}	V_0	V_{31}	V_0	V_{31}	V_0
-1	-1	V_7	V_8	V_9	V_{10}	V_1	V_2	V_3	V_4	V_5	V_6

Note: (V_1-V_{10})-virtual voltage vectors with magnitude of 0.553Vdc
(V_0, V_{31})-Actual null voltage vectors with zero magnitude

III. CONSTANT SWITCHING FLUX CONTROLLER DESIGN

A. Concept of Constant Switching Flux Controller

The proposed CSFHTC-DTC method uses a triangular-based constant switching flux (CSF) controller, a 3-level hysteresis torque controller, and a lookup table as shown in Fig. 4. The CSF controller produces the flux status (Ψ_{stat}) as 1,-1; and hysteresis torque controller torque status (T_{stat}) as 1, -1, and 0 respectively similar to classical DTC scheme.

The proposed 2-level CSF controller is implemented by using a triangular carrier wave ($C\Psi$), PI controller, and a comparator as shown in Fig. 5. The CSF controller gives output statuses (Ψ_{stat}) as +1 or -1 (means flux increment and decrement respectively) and forces to follow triangular carrier wave frequency as indicated in (12),

$$\begin{aligned} \Psi_{stat} &= 1 \quad \Psi_c \geq C_\Psi \\ \Psi_{stat} &= -1 \quad \Psi_c < C_\Psi \end{aligned} \quad (12)$$

Where Ψ_c = Output of the CSF PI controller
Ψ_{stat} = CSF controller output status

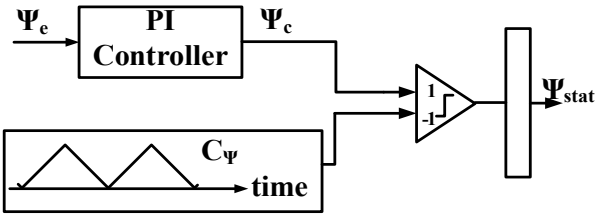

Fig. 5. 2-level constant switching flux (CSF) controller.

B. Design of Constant Switching Flux Controller

The stator flux slope depends on voltage vector magnitude and flux position as in (10) and (11). The average positive and negative slopes over a sector can be determined by assuming a constant slope during a stable flux state (Ψ_{stat}). The total number of positive or negative slopes in a sector can be expressed in terms of triangular carrier frequency and fundamental synchronous frequency as follows in (13).

$$N_f = \frac{2\pi f_{tri}}{10\omega_e} \quad (13)$$

Where N_f=total no. of negative/positive slopes in a sector
f_{tri}=triangular wave frequency(Hz)
ω_e=stator flux synchronous speed (rad/sec)
Total number of sectors of the flux locus=10

The average negative and average positive slope across a sector can be calculated from (10), (11), and (13).

$$\frac{d\Psi_s^-}{dt} = \frac{1}{N_f}\sum_{n=1}^{N_f}\frac{2}{5}v_{dc}\sin\left(\frac{\pi/5}{N_f}\right)n + \frac{2\pi}{5} = Q_\Psi \quad (14)$$

$$\frac{d\Psi_s^+}{dt} = \frac{1}{N_f}\sum_{n=1}^{N_f}\frac{2}{5}v_{dc}\sin\left(\frac{\pi/5}{N_f}\right)n = P_\Psi \quad (15)$$

The resultant average slope of stator flux from (14) and (15) will be written with CSF controller output duty ratio d_Ψ as below (16) and (17)

$$\frac{d\Psi_s}{dt} = P_\Psi d_\Psi + (1 - d_\Psi)Q_\Psi \quad (16)$$

$$\frac{d\Psi_s}{dt} = (P_\Psi - Q_\Psi)d_\Psi + Q_\Psi \quad (17)$$

With the introduction of perturbations in Ψ_s and d_Ψ, the open loop stator flux small signal transfer function can be achieved as in (18)

$$\frac{d\left(\Psi_s + \widehat{\Psi_s}\right)}{dt} = (P_\Psi - Q_\Psi)(d_\Psi + (\widehat{d_\Psi} + Q_\Psi) \quad (18)$$

Equating small signal linear terms on both sides in the above equation and applying Laplace transform, the flux loop transfer function with duty cycle can be written as (19)

$$\frac{\widehat{\Psi}_s}{\widehat{d}_\Psi} = \frac{P_\Psi - Q_\Psi}{S} \quad (19)$$

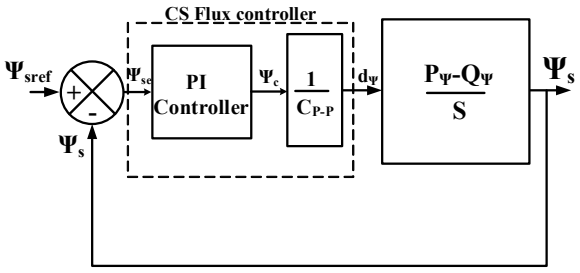

Fig. 6. Closed loop diagram of flux transfer function with CSF controller.

The closed-loop flux control diagram with the CSF controller and flux loop transfer function is shown in Fig. 6. Since the flux open loop transfer function contains an integral term with gain, the integral component of the PI controller for the flux loop is not necessary and the PI controller contains only proportional gain K_{pf}. The CS flux controller is designed such that the processed output of PI must not go beyond triangular carrier bounds.

There are two constraints to consider while designing the stator flux loop controller proportional gain K_{pf}.

- The PI controller's absolute slope must not be greater than the triangular carrier wave slope. From (10) and (11), the maximum positive and negative stator flux slopes occur at angles of π/5 and 0 during a sector respectively.

$$\text{The slope of triangular} >= \frac{2}{5} v_{dc} \sin\frac{\pi}{5} K_{pf} \quad (20)$$

The triangular carrier frequency chosen as 2500Hz with a peak-peak magnitude of 70 and hence the triangular carrier wave slope is 350000 sec^{-1}. The maximum positive and negative slopes for a DC voltage 125V can be obtained from (10) and (11) as 29.39, and -29.39 respectively. From (20), the proportional gain K_{pf} is obtained as < 11908.8.

- The closed loop stator flux transfer function bandwidth must not exceed half of the frequency of the triangular carrier wave

$$\frac{1}{2} f_{tri} \geq \text{BW(closed loop flux transfer function)} \quad (21)$$

From the second constraint (21), the K_{pf} is calculated by assuming the bandwidth of the closed loop transfer function should not be greater than half the triangular carrier wave frequency i.e. 1250Hz. The bandwidth of the closed-loop flux transfer function from Fig. 6 can be expressed by substituting the values listed in Table III

$$\left|\frac{0.52K_{pf}}{s + 0.52K_{pf}}\right|_{s=BW} = -3dB \quad (22)$$

Where, BW=Band width frequency in Rad/sec=2π(1250)

The critical value of the proportional gain K_{pf} of the CSF PI controller can be obtained from (22) by taking the bandwidth of the closed-loop flux control system as 2*π*1250 rad/sec and the obtained value of K_{pf} is 15178. The optimum value of K_{pf} can be selected by satisfying the above-mentioned two constraints i.e. $K_{pf} \leq 11908$.

The simulation test is performed with Matlab/Simulink software to test the effectiveness of the proposed CSFHTC-DTC method over the classical HFT-DTC method [18]. Fig. 7(a) and Fig. 7 (b) show the flux and torque pattern for a high speed of 1440 rpm for the HFT-DTC method and proposed CSFHTC-DTC respectively and observed that the proposed method improves the flux profile with the same torque profile. Similarly, Fig. 8 (a) and Fig. 8 (b) show the flux and torque response for the medium speed of 500rpm for the classical and proposed method respectively and it can be seen that the proposed method shows reduced flux ripple.

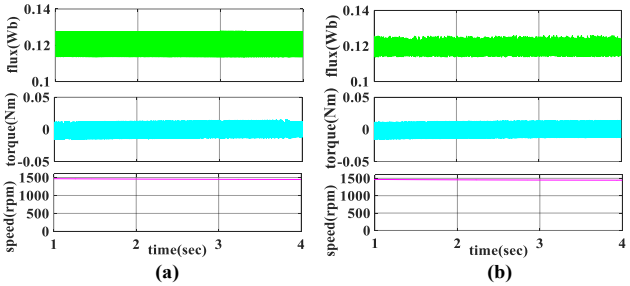

Fig. 7. Simulation results of stator flux, and torque patterns for a high speed of 1440 rpm (a) HFT-DTC (b) proposed CSFHTC-DTC.

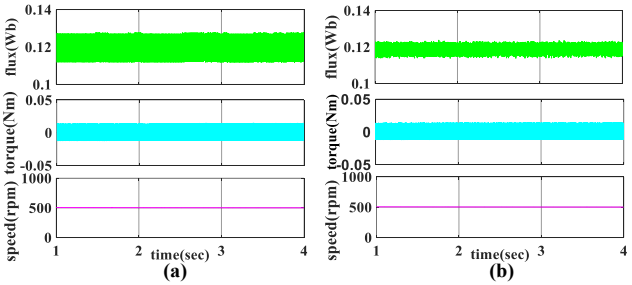

Fig. 8. Simulation results of stator flux, and torque patterns for a medium speed of 500 rpm (a) HFT-DTC (b) proposed CSFHTC-DTC.

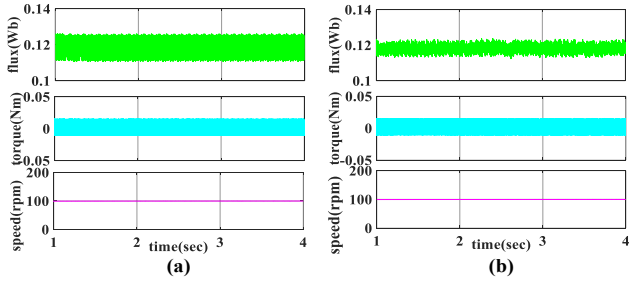

Fig. 8. Simulation results of stator flux, and torque patterns for a low speed of 100 rpm (a) HFT-DTC (b) proposed CSFHTC-DTC.

Fig. 9 (a) and Fig. 9 (b) show the response of torque and flux for a low speed of 100rpm and observed that great reduction of the flux ripple under low speeds.

The simulation results prove that the proposed constant CSF controller improves the flux ripple and in turn, improves the harmonic current %THD.

IV. Experimental Results Analysis

The novel constant switching flux controller and hysteresis torque controller-based DTC (CSFHTC-DTC) method is used for two-level inverter-controlled five-phase induction motor drives and is compared to the classical HFT-DTC scheme using experimental hardware results. The hardware setup for the proposed scheme is shown in Fig. 10. The hardware setup comprises a five-phase inverter power module with SEMIKRON IGBTs, DS1202 Micro Lab Box dSpace controller with control desk, 1024 PPR incremental speed sensor, 1 HP five-phase induction motor, separately excited DC Generator load, incandescent lamp load, 1-phase auto transformer, LEM makes LV 25-P voltage sensor and LA 25-P current sensors. For both the proposed CSFHTC-DTC and classical HFT-DTC approaches, the sample period for implementing the control algorithm is 100e-6 seconds. The HFT-DTC method [18] is implemented with the hysteresis torque band of 10% rated torque and flux band of 5% of reference flux. The five-phase machine parameters and control parameters are tabulated in Table III. The next sections analyze the hardware results of classical HFT-DTC and proposed CSFHTC-DTC techniques.

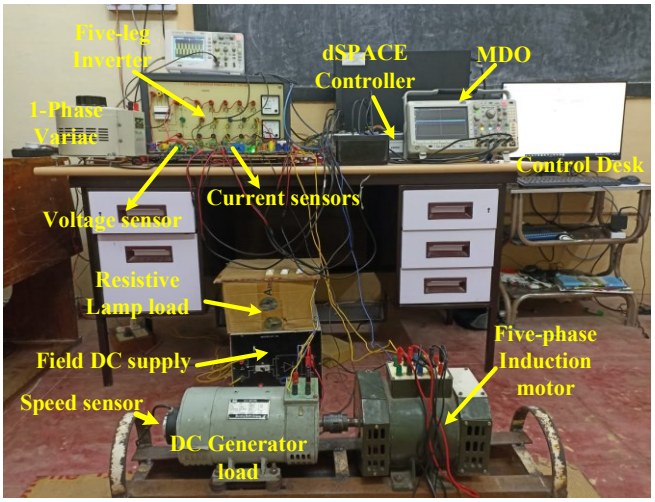

Fig. 10. The experimental hardware setup of a 2-level 5-phase inverter power module fed five-phase induction motor drive.

A. Steady-State Performance Analysis

The steady-state performance of a five-phase induction motor drive is examined for high speed (1440 rpm), medium speed (500 rpm), and low speed (100 rpm) under different loading situations to assess the efficacy of the suggested control method. The flux and torque ripples are computed by (23) from the acquired experimental data. The 10000 samples (N)/second data is taken for the computation of flux and torque ripples for the classical and proposed methods.

$$\text{Torque/Flux}_{\text{ripple}} = \sqrt{\frac{1}{N}\sum_{i=1}^{N}\left(X(i) - X_{\text{avg}}\right)^2} \tag{23}$$

Where X (i) =flux or torque during i^{th} sample

X_{avg}=average flux ripples or average torque ripple

1) Light load condition

Fig. 11 shows the stator flux and torque profiles for the speeds of 1440rpm,500rpm, and 100rpm for a light load/no load for the classical HFT-DTC method and found that classical HFT-DTC shows a torque ripple of 0.179Nm, 0.175Nm 0.166Nm and flux ripples of 0.0035Wb, 0.0035Wb, and 0.0036Wb respectively for the respective speeds. In Fig. 12, the proposed CSFHTC-DTC shows torque ripples of 0.173Nm, 0.179Nm, and 0.175Nm and flux ripples of 0.0015Wb, 00015Wb, and 0.0016Wb respectively for the speeds of 1440rpm, 500rpm, 100rpm respectively under light loads. From Fig. 11 and Fig. 12, it can be shown that the proposed CSFHTC-HTC shows a great decrement of 57% (approx.) in flux ripple for various operating speeds under light loads.

2) Loaded conditions

Fig. 13 presents the flux and torque patterns for the speeds of 1440rpm 500rpm and 100rpm under a load of 1.2 Nm for classical HFT-DTC and shows the torque ripples of 0.21Nm, 0.172Nm, and 0.166Nm; and flux ripples of 0.0035Wb, 0.0036Wb, and 0.0036Wb respectively. Fig. 14 shows the torque and flux patterns for the speeds of 1440rpm, 500rpm, and 100rpms under load of 1.2 Nm and observed that the proposed method exhibits torque ripples of 0.2Nm, 0.17Nm, and 0.17Nm; and flux ripples of 0.0015Wb, 0.0016Wb, and 0.0017Wb for the speeds of 1440rpm, 500rpm, 100rpm respectively.

From Fig. 13 and Fig. 14, it can be concluded that the proposed CSFHTC-DTC scheme shows a good reduction of average flux ripple without degrading the torque ripple as that of the classical HFT-DTC method for all variable speeds under loaded conditions.

3) The %THD performance analysis

The phase harmonic distortion is analyzed with various speeds at a load of 1.6 Nm for both classical and proposed methods. Fig. 15 shows the harmonic spectrum for a phase current under 1440 rpm at 1.6 Nm load and seen that the HFT-DTC gives a %THD of 23.8% whereas the CSFHTC-DTC shows a lower %THD of 17.82%.

Fig. 16 shows the harmonic spectrum for 500rpm at 1.6 Nm load for both HFT-DTC and the proposed CSFHTC-DTC method and the HFT-DTC shows a higher %THD of 34.14% whereas the CSFHTC-DTC shows a lower %THD of 28.34%. The harmonic spectrum for a low speed of 100rpm is shown in Fig. 17 and it can be observed that the HFT-DTC scheme exhibits a higher %THD of 43.8% whereas the proposed CSFHTC-DTC method gives a reduced %THD of 30.79%.

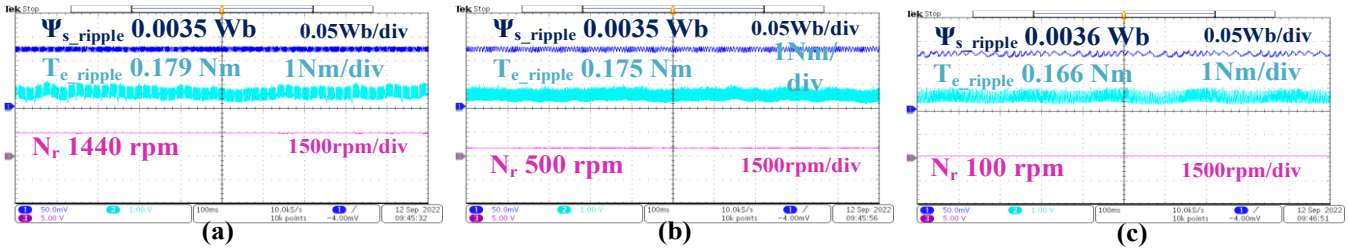

Fig. 11. Fux, torque patterns for speeds of (a) 1440rpm,(b) 500rpm, and (c) 100 rpm for classical HFT-DTC at light load/no load of 0.6Nm.

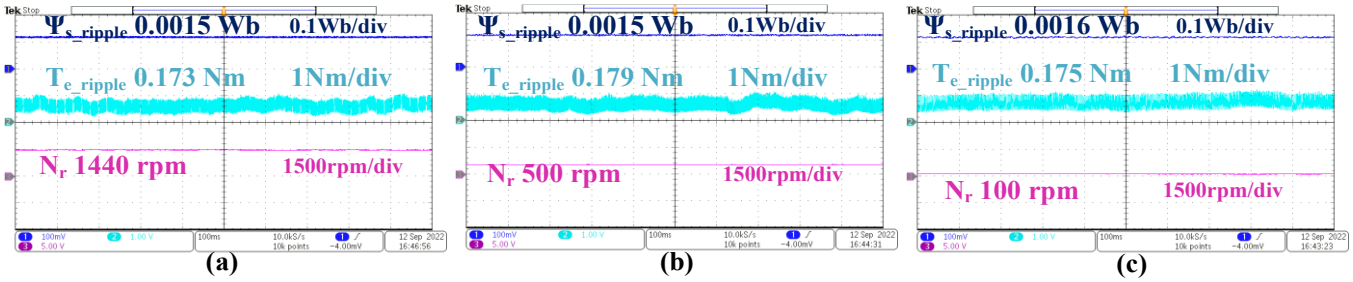

Fig. 12. Flux, torque patterns for speeds of (a)1440rpm, (b) 500rpm, and (c) 100 rpm for proposed CSFHTC-DTC at light load/no load of 0.6Nm.

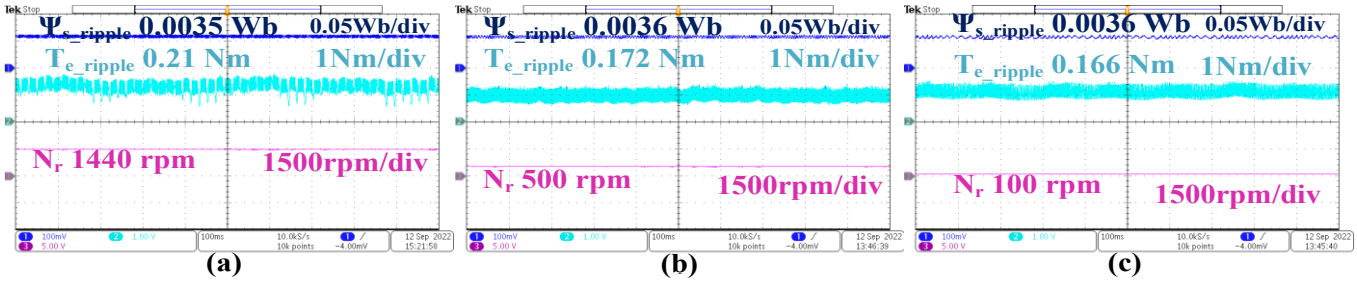

Fig. 13. Flux, torque patterns for speeds of (a) 1440rpm, (b) 500rpm, and (c) 100 rpm for classical HFT-DTC at a load of 1.2 Nm.

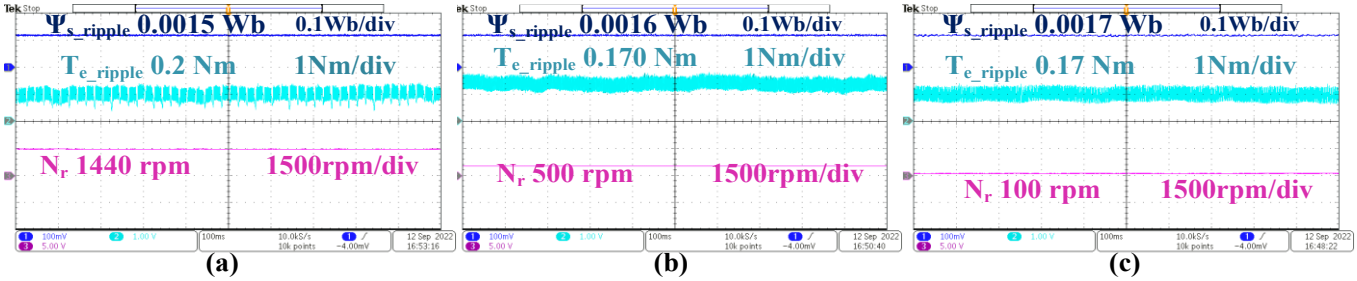

Fig. 14. Flux, torque patterns for speeds of (a) 1440rpm,(b) 500rpm, and (c) 100 rpm for classical CSFHTC-DTC at a load of 1.2 Nm.

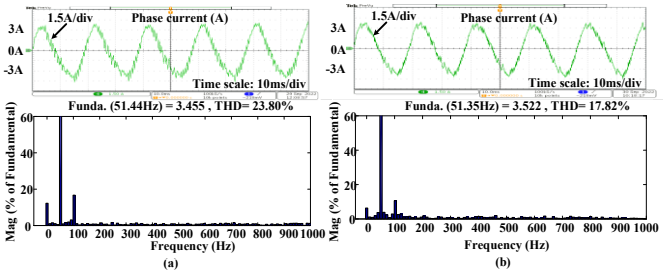

Fig. 15. Current %THD under load 1.6 Nm for 1440 rpm for (a) HFT-DTC and (b) CSFHTC-DTC method.

From Fig. 15, 16, and 17 it can be concluded that the CSFHTC-DTC improves the phase current profile. The current %THD improvement is due to the improved flux pattern as the current %THD depends on the flux profile.

Fig. 18 shows the fundamental (αβ) plane and harmonic (xy) plane currents for HFT-DTC and proposed CSFHTC-DTC methods for 1440 rpm at1.6 Nm load and it can be seen that the proposed method exhibits smooth fundamental currents and reduced harmonic plane xy currents.

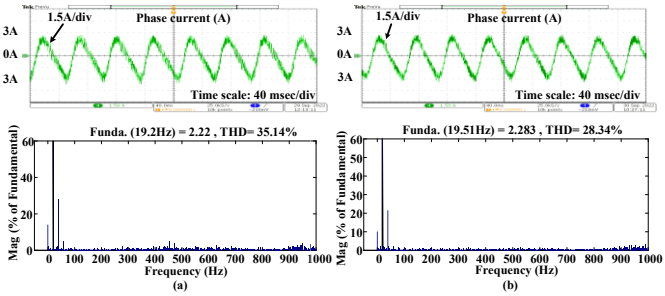

Fig. 16. Current %THD under load 1.6 Nm for 500 rpm for (a) HFT-DTC and (b) CSFHTC-DTC method

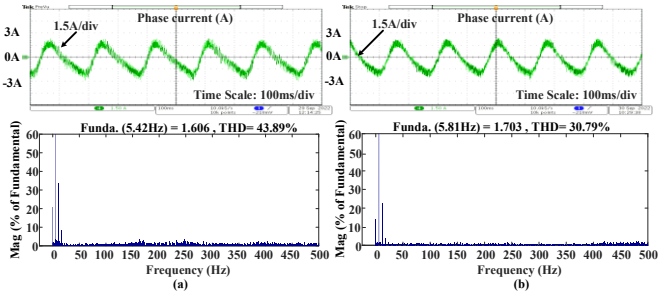

Fig. 17. Current %THD under load 1.6 Nm for 100 rpm for (a) HFT-DTC and (b) CSFHTC-DTC method.

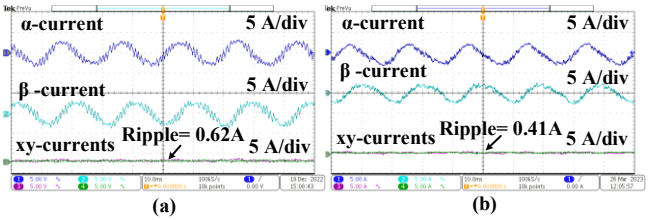

Fig. 18. Fundamental plane currents(α,β currents), harmonic plane currents (x,y currents) pattern for (a) HFT-DTC, (b) proposed CSFHTC-DTC.

B. *Analysis of Dynamic Performance*

The induction motor speed dynamics and torque dynamics are investigated below to evaluate the dynamic performance of classical HFT-DTC and novel CSFHTC-DTC schemes.

1) *Speed dynamics*

The speed dynamics of HFT-DTC and proposed CSFHTC-DTC methods are analyzed by creating speed disturbances as shown in Fig. 19 and the speed is changed from 500rpm-1000rpm-1400rpm.

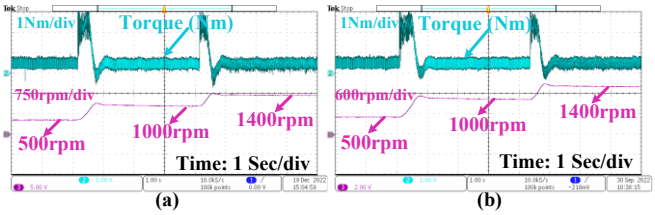

Fig. 19. Speed dynamic response for (a) HFT-DTC and (b) CSFHTC-DTC methods for 500rpm-1000rpm-1400rpm at light load.

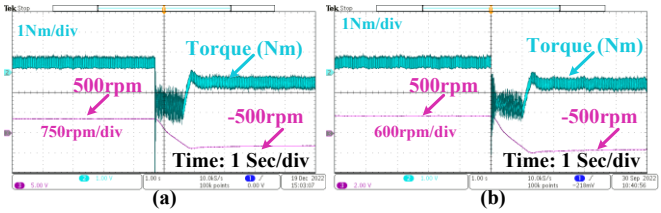

Fig. 20. Speed reversal response for (a) HFT-DTC and (b) CSFHTC-DTC methods from 500rpm to -500rpm at light load.

From Fig. 19, It is proved that the HFT-DTC and proposed CSFHTC-DTC scheme show the same speed response, and the proposed scheme won't disturb the actual speed dynamics. Fig. 20 depicts speed reversal disturbances changing from 500rpm to -500rpm for the HFT-DTC and CSFHTC-DTC schemes and both classical and proposed schemes show the same speed reversal dynamic performance.

2) *Torque dynamic analysis*

The torque dynamics are analyzed with sudden load disturbances at 1000rpm for both HFT-DTC and CSFHTC-DTC methods. The load disturbances are from 0.6Nm-1.2Nm-1.6Nm as in Fig. 21 and can be seen that both HFT-DTC and CSFHTC-DTC show the same type of torque transient response.

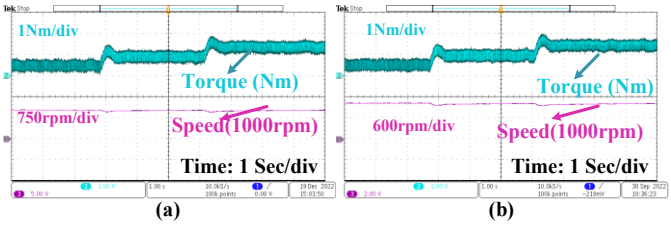

Fig. 21. Torque Dynamics 0.6 Nm-1.2Nm-1.6Nm at 1000rpm speed for (a) HFT-DTC and (b) CSFHTC-DTC method.

Fig. 22 shows the zoomed portion of speed dynamics (Fig. 19), speed reversal response (Fig. 20), and torque dynamics (Fig. 21) on the same plot for a fair comparison of the classical HFT-DTC and proposed CSFHTC-DTC scheme in terms of dynamics. From Fig. 22, it can be seen that the proposed CSFHTC-DTC scheme won't disturb the dynamic performance as that of the classical HFT-DTC scheme as the dynamics mainly depend on the torque controller.

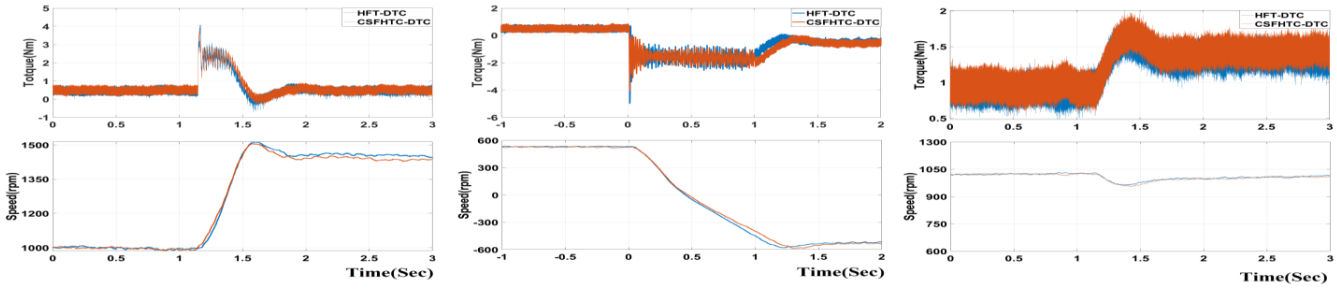

Fig. 22. Zoomed versions of speed dynamic Fig. 19 (left), speed reversal Fig. 20 (middle), and torque dynamic Fig. 21 (right) responses respectively for analyzing five-phase induction motor dynamics for HFT-DTC and proposed CSFHTC-DTC method.

C. *Comparative Results Analysis*

The average flux ripple, average torque ripple, harmonic distortion, and machine dynamics of the proposed CSFHTC-DTC scheme are analyzed with simulation and hardware results. The comparison Table II shows the average flux ripple and current harmonic distortion for high, medium, and low speeds for the no-load case and loaded cases for both methods.

From the comparison Table II, it can be concluded that

the proposed constant switching flux controller-based DTC scheme greatly improves the average flux ripple and current harmonic distortion without disturbing the average torque ripple and the fast dynamics and simplicity of the classical DTC scheme due to the usage of same hysteresis torque controller and lookup table. The machine parameters and controller parameters are tabulated in Table III.

TABLE II
COMPARATIVE RESULTS ANALYSIS TABLE FOR PROPOSED CSFHTC-DTC METHOD AND HFT-DTC METHOD

	Average flux ripple(Wb)						Current %THD		
Speed(rpm)	1400rpm		500rpm		100rpm		1400rpm	500rpm	100rpm
Load(Nm)	0.6Nm	1.2Nm	0.6Nm	1.2Nm	0.6Nm	1.2Nm	1.6Nm	1.6Nm	1.6Nm
HFT-DTC Method	0.0035	0.0035	0.0035	0.0036	0.0036	0.0036	23.8	35.14	43.89
CSFHTC-DTC Method	0.0015	0.0015	0.0015	0.0016	0.0015	0.0017	17.82	28.34	30.79
%Reduction	57.1	57.1	57.1	55.5	58.3	52.7	25.1	19.35	29.84

TABLE III
MACHINE PARAMETERS

Parameter	Value	Units
Power Rating	1	Horse Power(HP)
Stator resistance (Rs)	1.05	Ohms(Ω)
Stator inductance (Ls)	90.73	Milli Henry(mH)
Rotor resistance (Rr)	1.42	Ohm(Ω)
Rotor inductance (Lr)	90.73	Milli Henry(mH)
Mutual inductance (Lm)	84.73	Milli Henry(mH)
No. of Poles (P)	4	-
Rated Speed(Nr)	1440	rpm
P_Ψ, Q_Ψ values	18.11, -18.11	-
Speed PI controller	K_{ps}=0.02, K_{is}=0.005	-
CSF controller gain K_{pf}	11900	-

V. CONCLUSION

The proposed CSFHTC-DTC scheme uses the constant switching flux controller and hysteresis torque controller with the lookup table as in the classical HFT-DTC scheme of a five-phase induction motor. The proposed method exhibits a great improvement in average flux ripple and harmonic distortion of phase currents for various rotor speeds for lightly /no load and loaded cases. The proposed DTC exhibits fast dynamics as that of the classical HFT-DTC method and it won't disturb the simple structure of the classical one. As a whole, the suggested CSFHTC-DTC system is best suited for high power-density industrial applications where smooth operation and good dynamics are the primary limitations. The proposed method can be extended for both flux and torque controllers with multi-level inverter-controlled five-phase induction motors.

REFERENCES

[1] 'Multiphase induction motor drives – a technology status review' E. Levi, R. Bojoi, F. Profumo, H.A. Toliyat and S. Williamson IET Electr. Power Appl., 2007, 1, (4), pp. 489–516

[2] E. Levi, "Multiphase Electric Machines for Variable-Speed Applications," *in IEEE Transactions on Industrial Electronics*, vol. 55, no. 5, pp. 1893-1909, May 2008, doi: 10.1109/TIE.2008.918488.

[3] N. Bianchi, S. Bolognani and M. Dai Pre, "Strategies for the Fault-Tolerant Current Control of a Five-Phase Permanent-Magnet Motor," *in IEEE Transactions on Industry Applications*, vol. 43, no. 4, pp. 960-970, July-aug. 2007, doi: 10.1109/TIA.2007.900445.

[4] A. Tani, M. Mengoni, L. Zarri, G. Serra and D. Casadei, "Control of Multiphase Induction Motors With an Odd Number of Phases Under Open-Circuit Phase Faults," *in IEEE Transactions on Power Electronics*, vol. 27, no. 2, pp. 565-577, Feb. 2012, doi: 10.1109/TPEL.2011.2140334.

[5] M. Mengoni, L. Zarri, A. Tani, L. Parsa, G. Serra, and D. Casadei, "High-Torque-Density Control of Multiphase Induction Motor Drives Operating Over a Wide Speed Range," *in IEEE Transactions on Industrial Electronics*, vol. 62, no. 2, pp. 814-825, Feb. 2015, doi: 10.1109/TIE.2014.2334662.

[6] S. Williamson and S. Smith, "Pulsating torque and losses in multiphase induction machines," *Conference Record of the 2001 IEEE Industry Applications Conference. 36th IAS Annual Meeting* (Cat. No.01CH37248), Chicago, IL, USA, 2001, pp. 1155-1162 vol.2, doi: 10.1109/IAS.2001.955635.

[7] Wang, F.; Zhang, Z.; Mei, X.; Rodríguez, J.; Kennel, R. Advanced Control Strategies of Induction Machine: Field Oriented Control, Direct Torque Control and Model Predictive Control. *Energies* 2018, *11*, 120. https://doi.org/10.3390/en11010120

[8] A. Bhowate, M. V. Aware, and S. Sharma, "Predictive Torque Control Algorithm for a Five-Phase Induction Motor Drive for Reduced Torque Ripple With Switching Frequency Control," *in IEEE Transactions on Power Electronics*, vol. 35, no. 7, pp. 7282-7294, July 2020, doi: 10.1109/TPEL.2019.2954991.

[9] F. Barrero and M. J. Duran, "Recent Advances in the Design, Modeling, and Control of Multiphase Machines—Part I," *in IEEE Transactions on Industrial Electronics*, vol. 63, no. 1, pp. 449-458, Jan. 2016, doi: 10.1109/TIE.2015.2447733.

[10] M. J. Duran and F. Barrero, "Recent Advances in the Design, Modeling, and Control of Multiphase Machines—Part II," *in IEEE Transactions on Industrial Electronics*, vol. 63, no. 1, pp. 459-468, Jan. 2016, doi: 10.1109/TIE.2015.2448211.

[11] A. Baltatanu and M.L. Florea, "Multiphase machines used in electric vehicles propulsion," Proceedings of the International Conference on ELECTRONICS, COMPUTERS, and ARTIFICIAL INTELLIGENCE - ECAI-2013, 2013, pp. 1-6, doi: 10.1109/ECAI.2013.6636204.

[12] R. Bojoi, M. G. Neacsu, and A. Tenconi, "Analysis and survey of multi-phase power electronic converter topologies for the more electric aircraft applications," *International Symposium on Power Electronics, Electrical Drives, Automation and Motion, Sorrento*, Italy, 2012, pp. 440-445, doi: 10.1109/SPEEDAM.2012.6264566.

[13] I. Takahashi and T. Noguchi, "A New Quick-Response and High-Efficiency Control Strategy of an Induction Motor," *in IEEE Transactions on Industry Applications*, vol. IA-22, no. 5, pp. 820-827, Sept. 1986, doi 10.1109/TIA.1986.4504799.

[14] M. Bertoluzzo, G. Buja and R. Menis, "Analytical formulation of the direct control of induction motor drives," *ISIE '99. Proceedings of the IEEE International Symposium on Industrial Electronics* (Cat. No.99TH8465), 1999, pp. PS14-PS20 vol.1, doi: 10.1109/ISIE.1999.801745.

[15] V. Ambrozic, G. S. Buja and R. Menis, "Band-constrained technique for direct torque control of induction motor," *in IEEE Transactions on Industrial Electronics,* vol. 51, no. 4, pp. 776-784, Aug. 2004, doi:10.1109/TIE.2004.831722

[16] A. Iqbal and E. Levi, "Space vector modulation schemes for a five-phase voltage source inverter," *2005 European Conference on Power Electronics and Applications, Dresden, Germany*, 2005, pp. 12 pp.-P.12, doi: 10.1109/EPE.2005.219194.

[17] L. Parsa and H. A. Toliyat, "Sensorless Direct Torque Control of Five-Phase Interior Permanent-Magnet Motor Drives," *in IEEE Transactions on Industry Applications,* vol. 43, no. 4, pp. 952-959, July-aug. 2007, doi: 10.1109/TIA.2007.900444

[18] L. Zheng, J. E. Fletcher, B. W. Williams, and X. He, "A Novel Direct Torque Control Scheme for a Sensorless Five-Phase Induction Motor Drive," *in IEEE Transactions on Industrial Electronics*, vol. 58, no. 2, pp. 503-513, Feb. 2011, doi: 10.1109/TIE.2010.2047830.

[19] L. Gao, J. E. Fletcher, and L. Zheng, "Low-Speed Control Improvements for a Two-Level Five-Phase Inverter-Fed Induction Machine Using Classic Direct Torque Control," *in IEEE Transactions on Industrial Electronics,* vol. 58, no. 7, pp. 2744-2754, July 2011, doi: 10.1109/TIE.2010.2070775.

[20] J. A. Riveros, M. J. Durán, F. Barrero and S. Toral, "Direct torque control for five-phase induction motor drives with reduced common-mode voltage," *IECON 2012 - 38th Annual Conference on IEEE Industrial Electronics Society, Montreal, QC, Canada*, 2012, pp. 3616-3621, doi: 10.1109/IECON.2012.6389317.

[21] S. Payami and R. K. Behera, "An Improved DTC Technique for Low-Speed Operation of a Five-Phase Induction Motor," *in IEEE Transactions on Industrial Electronics,* vol. 64, no. 5, pp. 3513-3523, May 2017, doi: 10.1109/TIE.2017.2652397.

[22] Y. N. Tatte and M. V. Aware, "Torque Ripple and Harmonic Current Reduction in a Three-Level Inverter-Fed Direct-Torque-Controlled Five-Phase Induction Motor," *in IEEE Transactions on Industrial Electronics,* vol. 64, no. 7, pp. 5265-5275, July 2017, doi: 10.1109/TIE.2017.2677346.

[23] Yen-Shin Lai and Jian-Ho Chen, "A new approach to direct torque control of induction motor drives for constant inverter switching frequency and torque ripple reduction," *in IEEE Transactions on Energy Conversion*, vol. 16, no. 3, pp. 220-227, Sept. 2001, doi: 10.1109/60.937200.

[24] Atif Iqbal & Emil Levi (2006) Space Vector PWM Techniques for Sinusoidal Output Voltage Generation with a Five-Phase Voltage Source Inverter, Electric Power Components, and Systems, 34:2, 119-140, DOI: 10.1080/15325000500244427.

[25] N. R. N. Idris and A. H. M. Yatim, "Direct torque control of induction machines with constant switching frequency and reduced torque ripple," *in IEEE Transactions on Industrial Electronics*, vol. 51, no. 4, pp. 758-767, Aug. 2004, doi: 10.1109/TIE.2004.831718.

[26] G. H. B. Foo and X. Zhang, "Constant Switching Frequency Based Direct Torque Control of Interior Permanent Magnet Synchronous Motors With Reduced Ripples and Fast Torque Dynamics," *in IEEE Transactions on Power Electronics*, vol. 31, no. 9, pp. 6485-6493, Sept. 2016, doi: 10.1109/TPEL.2015.2503292.

[27] V. S. Reddy and S. Devabhaktuni, "Enhanced Low-Speed characteristics with Constant Switching Torque Controller-based DTC Technique of Five-Phase Induction Motor Drive with FOPI Control," *in IEEE Transactions on Industrial Electronics*, doi: 10.1109/TIE.2022.3227275.

[28] V. S. R. C and S. Devabhaktuni, "Low-speed Performance improvement of Constant Switching Frequency DTC of Five-Phase Induction Motor," 2021 *National Power Electronics Conference (NPEC), Bhubaneswar*, India, 2021, pp. 01-06, doi: 10.1109/NPEC52100.2021.9672519.

Venkata Subba reddy C was born in Kadapa, India in 1991. He received his Master's Degree (2015) in Power Electronics Drives from RGMCET Nandyal. Currently, he is working towards a Ph.D. degree from the Electrical Engineering Department, National Institute of Technology, Warangal, India. His current research work interests are speed control of multi-phase drives.

Swati Devabhaktuni received a Ph.D. degree in electrical engineering from the JNT University, Hyderabad in 2014. Currently, she is working as an Assistant professor at the National Institute of Technology, Warangal. Her research interests are power electronics, AC motor drives, and control system.